Research Square

Preprints are preliminary reports that have not undergone peer review.
They should not be considered conclusive, used to inform clinical practice,
or referenced by the media as validated information.

Targeted Isolation and Functional Characterization of Periganglionic Cardiac Telocytes

Jacques-Antoine Gemayel
Saint Joseph University
Youakim Saliba
Saint Joseph University
Christina Sahyoun
Université de Poitiers
Patrick Bois
Université de Poitiers
Aurelien Chatelier
Université de Poitiers
Nassim Fares
nassim.fares@usj.edu.lb

Saint Joseph University

Article

Keywords: Cardiac telocytes, intracardiac ganglia, intrinsic cardiac nervous system, neuro-stromal interactions, targeted cell isolation, calcium signaling

Posted Date: November 6th, 2026

DOI: https://doi.org/10.21203/rs.3.rs-11133300/v1

License: This work is licensed under a Creative Commons Attribution 4.0 International License.
Read Full License

Additional Declarations: No competing interests reported.

Targeted Isolation and Functional Characterization of Periganglionic Cardiac Telocytes

Jacques-Antoine Gemayel[1], Youakim Saliba[1], Christina Sahyoun[2], Patrick Bois[2], Aurelien Chatelier[2,3+], Nassim Fares[1+*]

[1] Laboratory of Research in Physiology and Pathophysiology, Faculty of Medicine, Saint Joseph University of Beirut, Beirut 1104 2020, Lebanon.
[2] PRéTI, Laboratory, UR 24184, University of Poitiers, 86000 Poitiers, France.
[3] CERVO Brain Research Centre, Faculty of Medicine, Université Laval, Québec City, QC G1J 2G3, Canada.
[+] Equivalent contribution *corresponding author

Abstract

Cardiac telocytes are specialized interstitial stromal cells implicated in tissue organization, intercellular communication, and cardiac remodeling. However, telocytes associated with the intrinsic cardiac nervous system remain poorly characterized, partly because of the lack of targeted isolation approaches. Here, we describe an optimized strategy for the isolation and functional characterization of telocyte-like cells from the intracardiac ganglionic region of the rat heart. Anatomically guided microdissection of the dorsal atrial ganglionic region was combined with sequential enzymatic dissociation and short-term primary culture. Isolated cells displayed characteristic telocyte-like morphology, including elongated cell bodies and moniliform telopodes with alternating podomers and podoms, and expressed the telocyte-associated markers CD34, PDGFRα, and vimentin. Immunofluorescence analysis further demonstrated elongated CD34-positive stromal cells within the connective tissue surrounding intracardiac ganglia. Functional competence was assessed using Fluo-4 AM-based intracellular Ca^{2+} imaging. Angiotensin II (1.4 μM) and caffeine (1.2 mM) significantly increased Ca^{2+}-dependent fluorescence ($P < 0.0001$ for both), with representative recordings showing a sustained post-peak response following angiotensin II stimulation and a faster, predominantly transient response following caffeine stimulation. Collectively, these findings establish an anatomically targeted approach for isolating functionally responsive periganglionic cardiac telocyte-like cells and provide an experimental platform for investigating telocyte biology and neuro-stromal interactions within the intrinsic cardiac nervous system.

Keywords: Cardiac telocytes; intracardiac ganglia; intrinsic cardiac nervous system; neuro-stromal interactions; targeted cell isolation; calcium signaling.

Introduction

Telocytes are a specialized population of interstitial stromal cells characterized by a small cell body and long, slender cytoplasmic processes termed telopodes. Telopodes display a characteristic moniliform appearance formed by alternating thin segments, known as podomers, and dilated regions, known as podoms[1,2]. Although cells with similar morphological features had previously been described in several tissues, the term "telocyte" was introduced in 2010 by Popescu and Faussone-Pellegrini to distinguish these cells from the classical interstitial cells of Cajal[2]. Since then, telocytes have been identified in numerous organs based on the combined assessment of their ultrastructure, morphology, immunophenotype, and anatomical distribution[1,3]. Transmission electron microscopy remains the reference method for detailed ultrastructural characterization, although characteristic telopode-like structures can also be visualized using phase-contrast, fluorescence, and confocal microscopy[1,3].

Within the heart, telocytes have been reported in multiple anatomical compartments, including the epicardium, atrial and ventricular myocardium, endocardium, cardiac valves, and perivascular regions[4,5]. Cardiac telocytes form interconnected stromal networks and establish close spatial relationships with cardiomyocytes, endothelial cells, fibroblasts, immune cells, progenitor cells, and nerve fibers[5]. These associations have led to proposed roles in intercellular communication, extracellular matrix organization, tissue homeostasis, angiogenesis, repair, and fibrotic remodeling[4,5]. Telocytes may communicate with neighboring cells through direct membrane contacts, paracrine mediators, and extracellular vesicles[5,6]. Nevertheless, many of their proposed cardiac functions remain incompletely defined, partly because these cells are difficult to isolate and distinguish from other cardiac stromal populations.

No single molecular marker is currently considered specific for cardiac telocytes. Their characterization therefore relies on the integration of characteristic morphology, anatomical localization, and the expression of stromal markers such as CD34, platelet-derived growth factor receptor alpha (PDGFRα), platelet-derived growth factor receptor beta (PDGFRβ), and vimentin[7–9]. This multimodal characterization strategy is particularly important because several of these markers may also be expressed by other stromal and vascular cell populations[7–9]. In addition to their distinctive morphology, telocytes from several organs have been shown to exhibit intracellular Ca^{2+} signaling, which may contribute to cellular processes including secretion, mechanosensing, and communication with surrounding cells[10]. However, calcium signaling in cardiac telocytes, particularly those originating from anatomically specialized neurocardiac regions, remains insufficiently characterized[10,11].

Previous cardiac telocyte isolation protocols have generally relied on enzymatic digestion of myocardial tissue followed by culture, differential adhesion, immunophenotypic characterization, or cell-sorting approaches[7–9]. Although these approaches have contributed substantially to the characterization of cardiac telocytes, they may generate heterogeneous cell suspensions containing fibroblasts, endothelial cells, vascular smooth muscle cells, immune cells, and other stromal populations. In addition, extensive tissue digestion and mechanical dissociation may compromise cellular integrity and the capacity of isolated cells to preserve or re-establish their delicate telopodal morphology. Moreover, isolation from broad myocardial regions limits precise determination of the anatomical microenvironment from which individual

telocytes originate. The limited availability of targeted methods for isolating telocytes from anatomically defined cardiac regions therefore limits the investigation of potential regional differences in telocyte phenotype and function.

Intrinsic cardiac ganglia are concentrated predominantly within atrial ganglionated plexuses and represent major components of the intrinsic cardiac nervous system[12–14]. These ganglia comprise neuronal cell bodies, autonomic nerve fibers, glial cells, vascular structures, extracellular matrix, and diverse stromal cell populations[12–14]. Through the local integration and modulation of autonomic signals, the intrinsic cardiac nervous system contributes to the regulation of heart rate, conduction, contractility, and regional cardiac function[12,13]. Despite the specialized organization of this neurocardiac microenvironment, periganglionic cardiac telocytes have not been systematically isolated and functionally characterized as a regionally derived cell population.

We hypothesized that targeted microdissection of the ganglion-containing dorsal atrial region could provide an anatomically defined source of periganglionic cardiac telocytes while enabling assessment of their characteristic structural and functional properties in culture. Accordingly, this study aimed to develop and evaluate a targeted isolation protocol for periganglionic cardiac telocytes from the rat intracardiac ganglionic region. Isolated cells were assessed using complementary morphological and immunophenotypic approaches, while their anatomical context was examined by confocal imaging of cardiac tissue. Functional responsiveness was further evaluated using live-cell calcium imaging following stimulation with angiotensin II and caffeine. This anatomically guided approach establishes a region-specific experimental platform for studying telocytes associated with the intrinsic cardiac nervous system and may support future investigations of neuro-stromal communication and cardiac remodeling.

Materials and Methods

1. Animals

This study was approved by the Ethics Committee of Saint Joseph University of Beirut (approval no. USJ-2023-314). All animal procedures were conducted in accordance with the *Guiding Principles for the Care and Use of Animals* established by the American Physiological Society, the *Guide for the Care and Use of Laboratory Animals* of the National Institutes of Health, and European Parliament Directive 2010/63/EU. Euthanasia procedures were conducted in accordance with the *AVMA Guidelines for the Euthanasia of Animals: 2020 Edition*.

Sixteen adult male Wistar rats, approximately 4 months of age and weighing 240–280 g, were obtained from an established breeding colony maintained at Saint Joseph University of Beirut. The colony was originally established from Wistar rats purchased from Janvier Labs (Le Genest-Saint-Isle, France) and has subsequently been maintained through in-house breeding. Animals were maintained under controlled temperature and humidity conditions, provided with standard rodent chow and ad libitum access to tap water, and acclimatized before experimental procedures.

Of the sixteen animals, six were used for cell isolation, morphological characterization, immunophenotyping, viability assessment, and short-term culture experiments; eight were used

for intracellular calcium-imaging experiments; and two were used for qualitative regional CD34 mapping.

2. Anesthesia, Heart Extraction, and Ganglionic Region Microdissection

Rats were deeply anesthetized by intramuscular administration of ketamine hydrochloride (75 mg/kg; Interchemie, Waalre, the Netherlands) and xylazine hydrochloride (10 mg/kg; Rotexmedica, Trittau, Germany). Adequate depth of anesthesia was confirmed by the absence of the pedal withdrawal reflex.

Following confirmation of deep anesthesia, a median thoracotomy was performed. While maintained under deep anesthesia, the animals were euthanized by bilateral thoracotomy followed by exsanguination through heart excision. The heart was rapidly excised and immediately transferred to ice-cold Ca^{2+}- and Mg^{2+}-free Hanks' balanced salt solution (HBSS). The euthanasia procedure was performed in accordance with the *AVMA Guidelines for the Euthanasia of Animals: 2020 Edition*.

The HBSS contained 140 mM NaCl, 5 mM KCl, 0.3 mM Na_2HPO_4, 0.4 mM KH_2PO_4, 6 mM glucose, 4 mM $NaHCO_3$, and 10 mM HEPES and was supplemented with 1% penicillin–streptomycin. The pH was adjusted to 7.42 and the osmolarity to approximately 305 mOsm.

The heart was rinsed several times in ice-cold Ca^{2+}- and Mg^{2+}-free HBSS to remove residual blood and was maintained in the same solution during microdissection. The heart was positioned with its dorsal surface facing upward, and the dorsal atrial fat-pad region between the atrial appendages was identified under a stereomicroscope. Intracardiac ganglia were identified as small, pale nodular structures embedded within the dorsal atrial connective and adipose tissue and associated with visible nerve fibers.

The ganglion-containing fat-pad region was carefully microdissected together with a thin rim of surrounding stromal tissue (Fig. 1). This targeted dissection was performed to retain the periganglionic microenvironment while minimizing contamination by atrial and ventricular myocardium. Ganglion-containing tissue obtained from each heart was pooled and immediately transferred to fresh ice-cold Ca^{2+}- and Mg^{2+}-free HBSS.

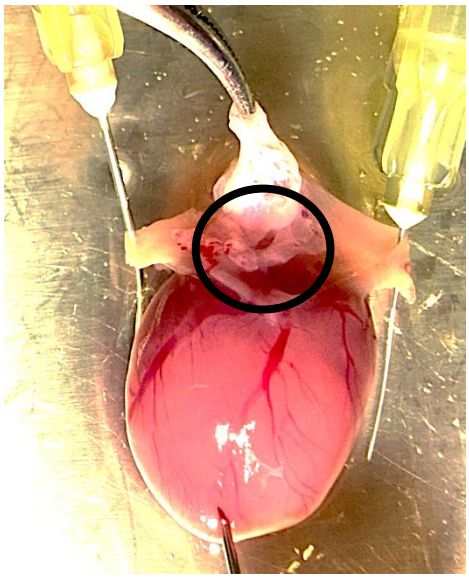


Figure 1. *Whole-heart dorsal view showing the intracardiac ganglionic region located between the atrial appendages (black circle).*

3. Tissue Fragmentation and Enzymatic Dissociation

The dissociation procedure was adapted from the neuronal isolation method described by Lizot et al. (2022)[14], with modifications intended to facilitate the recovery of perignanglionic stromal cells while maintaining cellular viability.

Dissected tissue was cut into fragments of approximately 0.5–1 mm^3 using fine scissors. Tissue fragments were transferred into 2 mL of Ca^{2+}- and Mg^{2+}-free HBSS containing collagenase type II at a final concentration of 3 mg/mL (Worthington Biochemical Corporation, Lakewood, NJ, USA), Dispase II at 7.5 mg/mL (Sigma-Aldrich, Lyon, France), and DNase I at 0.25 mg/mL (Sigma-Aldrich, Lyon, France). Samples were incubated for 30 min at 37°C with gentle agitation.

Following the first digestion step, tissue fragments were transferred into 2 mL of 0.25% trypsin-EDTA supplemented with DNase I (0.25 mg/mL) and incubated for an additional 35 min at 37°C. Enzymatic activity was terminated by adding an equal volume of Dulbecco's Modified Eagle Medium (DMEM; Sigma-Aldrich, catalogue no. D6046) supplemented with 10% fetal bovine serum (FBS). Tissue fragments were then washed twice with complete culture medium before mechanical dissociation.

4. Mechanical Trituration

Following enzymatic dissociation and washing, tissue fragments were gently triturated using a sequential series of three fire-polished glass Pasteur pipettes with progressively smaller bore diameters. Before use, the pipettes were coated with serum-containing medium to reduce nonspecific cellular adhesion to the glass surface. Trituration was performed slowly to avoid

bubble formation and excessive mechanical shear. Large residual tissue fragments were allowed to settle briefly, and the cell-containing supernatant was collected for plating.

5. Cell Plating and Culture Conditions

Cells were resuspended in complete DMEM supplemented with 10% FBS, 2 mM L-glutamine, and 1% penicillin–streptomycin (Cat. No. MS01YE1006). The cell suspension was plated as small droplets onto 35-mm glass-bottom culture dishes coated overnight with poly-D-lysine at 1.0 mg/mL (Merck Millipore, Burlington, MA, USA; Cat. No. A-003-E) and subsequently with laminin at 10 µg/mL (Roche, Mannheim, Germany; Cat. No. 11243217001) overnight at 4°C. Cells were incubated for 3–5 h at 37°C in a humidified atmosphere containing 5% CO_2. Complete culture medium was then gently added to obtain a final volume of 2 mL per dish.

Cultures were maintained as primary passage-zero preparations and were not passaged. Morphological characterization, immunofluorescence, viability assessment, and calcium-imaging experiments were performed between 72 and 96 h after plating.

6. Control of Fibroblast-Like Cell Proliferation

Cytosine β-D-arabinofuranoside (Ara-C; Sigma-Aldrich, catalogue no. C-1768) was evaluated as an optional antimitotic treatment in selected short-term culture-stability experiments. Following the initial cellular attachment period, Ara-C was added to the culture medium at a final concentration of 10 µM and maintained for up to 96 h. Parallel cultures maintained under identical conditions without Ara-C served as controls. Cultures were examined after 48 and 96 h using phase-contrast microscopy, propidium iodide staining, and Trypan blue exclusion.

7. Morphological Characterization of Isolated Telocyte-Like Cells

Cultured cells were examined by phase-contrast microscopy using a VaNgUARD high-definition digital camera (VEE GEE Scientific, Illinois, USA). Telocyte-like cells were morphologically characterized by a small spindle-shaped, oval, or piriform cell body and one or more long, thin, moniliform cytoplasmic processes consistent with telopodes. Cells displaying broad or flattened cell bodies with relatively short, thick cytoplasmic processes and lacking recognizable moniliform telopodes were classified as fibroblast-like and excluded from telocyte-specific analyses.

Morphological characterization was subsequently integrated with immunophenotypic assessment and anatomical origin because no individual molecular marker is considered specific for telocytes.

8. Immunofluorescence Staining of Cultured Telocyte-Like Cells

Cultured cells were fixed with 4% paraformaldehyde for 20 min at 4°C, washed three times with phosphate-buffered saline (PBS), permeabilized with 0.5% Triton X-100 for 20 min at room temperature, and blocked for 1 h at room temperature in PBS containing 10% goat serum and 1% bovine serum albumin (BSA).

Cells were subsequently incubated overnight at 4°C with the primary antibodies listed in Table 1. After three washes with PBS, cells were incubated for 30 min at room temperature in the dark with the appropriate fluorescent secondary antibodies listed in Table 1 at a dilution of 1:500. Nuclei were counterstained with DAPI (Table 1) for 10 min. Samples were mounted using Mowiol mounting solution and stored at 2–8°C protected from light until imaging.

Negative-control samples were processed in parallel by omitting the primary antibodies. Confocal images were acquired using an Olympus FV3000 laser-scanning confocal microscope (Olympus Corporation, Tokyo, Japan). Telocyte-like cells were characterized by integrating their elongated moniliform morphology with immunoreactivity for CD34, PDGFRα, and vimentin.

9. Immunofluorescence Staining of Intracardiac Ganglia

Cryosections (40–50 μm) containing the dorsal atrial region and intracardiac ganglia were permeabilized with 0.5% Triton X-100 for 20 min at room temperature and blocked for 1 h at 37°C in PBS containing 10% goat serum and 1% BSA.

Sections were incubated overnight at 4°C with the primary antibodies listed in Table 1, washed five times with PBS (1 min per wash), and incubated for 30 min at 37°C in the dark with the appropriate fluorescent secondary antibodies listed in Table 1 at a dilution of 1:500. Nuclei were counterstained with DAPI (Table 1) for 10 min. Sections were mounted using Mowiol mounting solution and stored protected from light until imaging.

Negative-control sections were processed in parallel by omitting the primary antibodies. Confocal imaging was performed using an Olympus FV3000 laser-scanning confocal microscope (Olympus Corporation, Tokyo, Japan). Z-stack images were acquired using a 20× objective with a 2× digital zoom to visualize the spatial relationships among CD34-positive stromal cells, PGP9.5-positive intrinsic cardiac neurons and nerve fibers, and α-smooth muscle actin (α-SMA)-positive vascular structures.

Table 1. Antibodies and nuclear counterstain used for immunofluorescence staining

Reagent/Target	*Supplier*	*Catalogue No.*	*Host/Specificity*	*Clone*	*Fluorophore*	*Working dilution*
Primary antibodies						
CD34	R&D Systems (Minneapolis, MN, USA)	AF4117	Goat	Polyclonal	—	1:150
PDGFRα	Santa Cruz Biotechnology (Dallas, TX, USA)	Sc-398206	Mouse	Monoclonal	—	1:200
Vimentin	ABclonal Technology (Woburn, MA, USA)	A19607	Rabbit	Polyclonal	—	1:100
PGP9.5	Merck–Sigma-Aldrich (St.	AB1761-I	Rabbit	Polyclonal	—	1:1,000

	Louis, MO, USA)					
α-Smooth Muscle Actin (ACTA2)	Sigma-Aldrich (St. Louis, MO, USA)	A2547	Mouse	1A4	—	1:100
Secondary antibodies						
Donkey anti-Goat	Invitrogen, Thermo Fisher Scientific	A11055	Donkey anti-Goat	—	Alexa Fluor 488	1:500
Donkey anti-Goat	Invitrogen, Thermo Fisher Scientific	A21432	Donkey anti-Goat	—	Alexa Fluor 555	1:500
Donkey anti-Goat	Invitrogen, Thermo Fisher Scientific	A21447	Donkey anti-Goat	—	Alexa Fluor 647	1:500
Chicken anti-Rabbit	Invitrogen, Thermo Fisher Scientific	A21441	Chicken anti-Rabbit	—	Alexa Fluor 488	1:500
Donkey anti-Rabbit	Invitrogen, Thermo Fisher Scientific	A31572	Donkey anti-Rabbit	—	Alexa Fluor 555	1:500
Donkey anti-Rabbit	Invitrogen, Thermo Fisher Scientific	A31573	Donkey anti-Rabbit	—	Alexa Fluor 647	1:500
Chicken anti-Mouse	Invitrogen, Thermo Fisher Scientific	A21200	Chicken anti-Mouse	—	Alexa Fluor 488	1:500
Donkey anti-Mouse	Invitrogen, Thermo Fisher Scientific	A31571	Donkey anti-Mouse	—	Alexa Fluor 647	1:500
Nuclear counterstain						
DAPI	Sigma-Aldrich	D9542	Nuclear DNA stain	—		

10. Representative Regional Mapping of CD34-Positive Cells

Representative regional CD34 mapping was performed using longitudinal cryosections obtained from two rat hearts. Sections encompassing the intracardiac ganglionic region, non-ganglionic atrial myocardium, upper ventricular myocardium, lower ventricular myocardium, and cardiac apex were collected at a thickness of 40–50 µm. Sections were processed for CD34 immunofluorescence and DAPI nuclear counterstaining using the staining conditions described above. Representative images were acquired using a 20× objective under identical confocal acquisition settings for all anatomical regions. This analysis was qualitative and was performed to illustrate the anatomical distribution of elongated CD34-positive interstitial cells throughout the rat heart. No regional cell-density quantification or inferential statistical comparison was performed.

11. Assessment of Cell Viability and Membrane Integrity

Cell viability was evaluated using Trypan blue exclusion and propidium iodide (PI) staining in cultures prepared separately from those used for intracellular calcium imaging. For the Trypan blue exclusion assay, cells were incubated with 0.4% Trypan blue solution prepared in phosphate-buffered saline (Sigma-Aldrich, St. Louis, MO, USA). Trypan blue-positive and Trypan blue-negative cells were counted using a hemocytometer under light microscopy. Cells excluding the dye were considered viable, whereas blue-stained cells were considered non-viable. Cell viability was calculated as follows:

Cell viability (%) = (number of Trypan blue-negative cells / total number of cells) × 100.

To further assess plasma membrane integrity, parallel cultures were incubated with propidium iodide (3 μM in complete culture medium). PI fluorescence was detected at an emission wavelength of 620 nm using fluorescence microscopy. Cells lacking nuclear PI fluorescence were considered to have preserved plasma membrane integrity, whereas cells exhibiting nuclear PI fluorescence were considered non-viable.

Viability was assessed immediately after isolation and after 48 and 96 h of culture in selected untreated and Ara-C-treated preparations. These assays were used as representative measures of short-term culture viability and membrane integrity. Separate culture dishes were used for viability assessment and intracellular calcium-imaging experiments.

12. Intracellular Calcium Imaging

Intracellular calcium dynamics were assessed using the calcium-sensitive fluorescent indicator Fluo-4 AM (Molecular Probes, Thermo Fisher Scientific, MA, USA). Cultured cells were incubated with 4 μM Fluo-4 AM for 15 min at 37°C in the dark. Following loading, cells were washed with calcium-containing Tyrode solution and maintained in Tyrode solution for 5 min to establish a stable prestimulation baseline before pharmacological stimulation.

The Tyrode solution contained 140 mM NaCl, 5.7 mM KCl, 1.7 mM $MgCl_2$, 2 mM $CaCl_2$, 4.4 mM $NaHCO_3$, 1.5 mM KH_2PO_4, 10 mM HEPES, 10 mM creatine monohydrate, 20 mM taurine, and 11.7 mM D-glucose. The pH was adjusted to 7.2 using NaOH.

Fluorescence imaging was performed using an InCyt Im2 digital fluorescence-imaging system (Intracellular Imaging Inc., Cincinnati, OH, USA) equipped with a 20× Super Fluor objective. Fluo-4 was excited at 488 nm, and fluorescence emission was collected using the corresponding filter set. Live-cell fluorescence imaging was performed at room temperature (25°C), with images acquired at 2 frames/s. Recording was continued following agonist application for a total experimental duration of approximately 10 min.

Cells were selected for analysis according to the predefined morphological criteria described above, including a compact cell body and one or more long, thin, telopode-like processes. Rounded cells and cells displaying broad cell bodies with short, thick processes were excluded from the analysis.

Regions of interest were manually drawn around individual cells using InCyt Im2 software. Background fluorescence was subtracted using a cell-free region from the same imaging field. For each analyzed cell, prestimulation baseline fluorescence and maximal post-stimulation fluorescence were extracted using the same analysis procedure.

For paired baseline and post-stimulation analyses, fluorescence amplitudes were expressed in arbitrary units (a.u.). For visualization of temporal calcium responses, fluorescence signals were normalized to the prestimulation baseline (F_0) and expressed as F/F_0. For comparison of normalized response amplitudes, changes in fluorescence relative to baseline were expressed as $\Delta F/F_0$, where $\Delta F = F - F_0$. The same processing and normalization procedures were applied to all cellular measurements within each pharmacological experiment.

Calcium-imaging experiments were performed using cultures derived from eight independent animals.

13. Angiotensin II and Caffeine Stimulation

Angiotensin II (Tocris Bioscience, Bio-Techne, catalogue no. 1158, Abingdon, UK) was prepared as a 1 mM stock solution in deionized water and applied at a final concentration of 1.4 μM. Angiotensin II-evoked responses were assessed by comparing prestimulation fluorescence with the corresponding maximal post-stimulation fluorescence in the same cell. A total of 46 paired cellular measurements obtained from cultures derived from eight independent animals were included in the final analysis.

Caffeine (ReagentPlus®, Sigma-Aldrich, catalogue no. C0750-100G) was prepared as a 1 M stock solution in deionized water and applied at a final concentration of 1.2 mM. Caffeine-evoked responses were assessed by comparing prestimulation fluorescence with the corresponding maximal post-stimulation fluorescence in the same cell. A total of 21 paired cellular measurements obtained from cultures derived from eight independent animals were included in the final analysis.

Cells cultured on 35-mm glass-bottom dishes were perfused with the different solutions using a ValveLink 8.2 Perfusion Controller (Automate Scientific, CA, USA). Solutions were removed at 3-min intervals using an Instech P720 peristaltic pump (Instech Laboratories, PA, USA). Because both angiotensin II and caffeine stock solutions were prepared in deionized water, control recordings were performed using Tyrode solution under the same perfusion conditions.

14. Statistical Analysis

Statistical analyses were performed using GraphPad Prism version 10.3.1 (GraphPad Software, San Diego, CA, USA). Data are presented as mean ± standard error of the mean (SEM), unless otherwise indicated. Statistical significance was defined as $P < 0.05$.

For intracellular calcium-imaging experiments, paired prestimulation and post-stimulation fluorescence measurements were obtained from the same individual cells. Angiotensin II experiments included 46 cells and caffeine experiments included 21 cells, with cells obtained

from cultures derived from eight independent animals in each experiment. Individual cells constituted the observational units for the paired cellular-response analyses. The number of analyzed cells and the number of contributing animals are reported for each experiment.

Normality of the paired differences between prestimulation and post-stimulation measurements was assessed using the Shapiro-Wilk test. Normally distributed paired differences were analyzed using a paired t-test, whereas non-normally distributed paired differences were analyzed using the Wilcoxon matched-pairs signed-rank test. For both angiotensin II and caffeine experiments, the paired differences deviated significantly from normality; therefore, Wilcoxon matched-pairs signed-rank tests were used for the final paired comparisons.

Representative regional CD34 mapping was performed as a qualitative anatomical assessment and was therefore not subjected to inferential statistical analysis.

RESULTS

1. Morphological Characterization of Isolated Telocyte-Like Cells

Telocyte-like cells were successfully obtained from all animals used for cell-isolation and morphological characterization experiments (n = 6). Following plating, cells adhered to the culture surface and progressively displayed morphological features consistent with telocytes in primary culture. Phase-contrast microscopy revealed cells with small spindle-shaped, oval, or piriform cell bodies giving rise to one or more long, thin, moniliform cytoplasmic processes consistent with telopodes (Fig. 2).

These processes extended over several cell diameters and frequently established contacts with neighboring telocyte-like cells, resulting in interconnected cellular networks. Higher-magnification imaging revealed alternating thin segments (podomers) and dilated regions (podoms) along the telopode-like processes. Variability in process length and branching was observed among individual cells, while the overall telocyte-like morphological phenotype was observed across all six independent preparations.

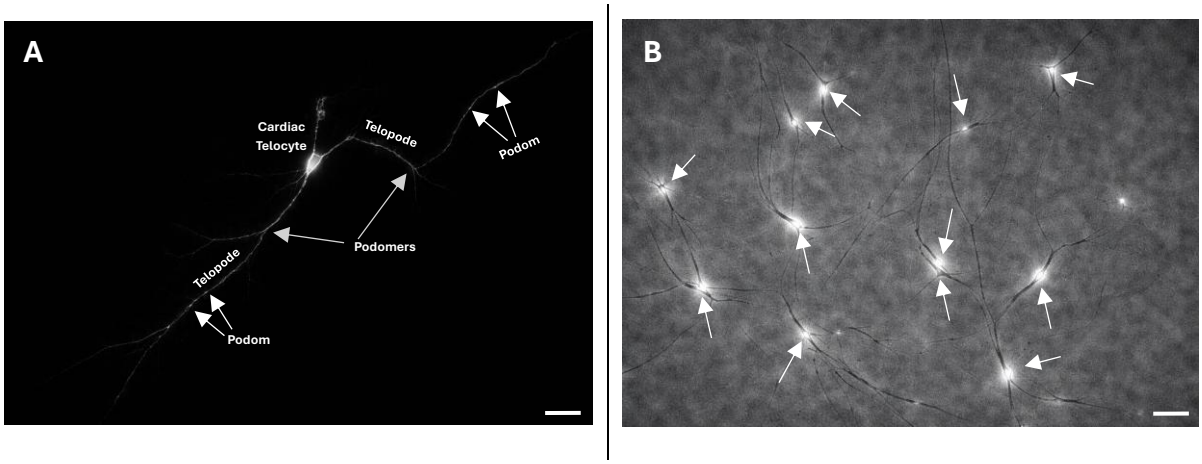


Figure 2. Morphological characterization of isolated periganglionic cardiac telocyte-like cells in primary culture. **(A)** Representative phase-contrast image of an isolated cardiac telocyte displaying a small cell body and long, thin moniliform telopodes. Arrows indicate alternating podomers and podoms. **(B)** Representative network of interconnected cardiac telocye-like cells showing extensive telopode branching and cellular contacts. Arrows indicate telopodes and telopode–telopode contacts. All images were acquired using a 20× objective. Scale bars = 20 µm.

2. Immunophenotypic Characterization of Isolated Cardiac Telocyte-like Cells

To further characterize the isolated telocyte-like cells, immunofluorescence staining was performed for the telocyte-associated markers CD34, PDGFRα, and vimentin. Positive immunoreactivity for each marker was observed in cells displaying the characteristic telocyte-like morphology, including compact cell bodies and elongated cytoplasmic processes (Fig. 3).

CD34 immunoreactivity was observed in elongated cells exhibiting the morphological features identified by phase-contrast microscopy. PDGFRα immunoreactivity was detected in the cell body and along elongated cellular processes. Vimentin immunoreactivity was also observed in cells displaying the characteristic elongated morphology, supporting their mesenchymal phenotype. Together, these findings demonstrated that the morphologically identified telocyte-like cells expressed CD34, PDGFRα, and vimentin. DAPI counterstaining confirmed intact nuclear morphology in all preparations.

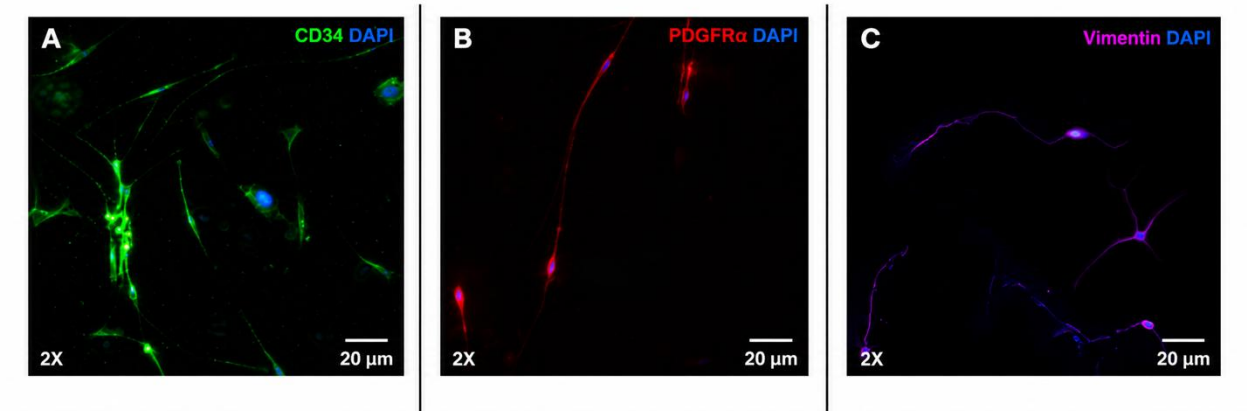


Figure 3. Immunophenotypic characterization of isolated cardiac telocyte-like cells. Representative immunofluorescence images of cultured cardiac telocyte-like cells labeled for **(A)** CD34, **(B)** PDGFRα, and **(C)** Vimentin, with DAPI nuclear counterstaining. Positive immunoreactivity was observed in cells displaying small cell bodies and elongated telopode-like cytoplasmic processes. Images were acquired using a 20× objective with a 2× digital zoom. Scale bars = 20 µm.

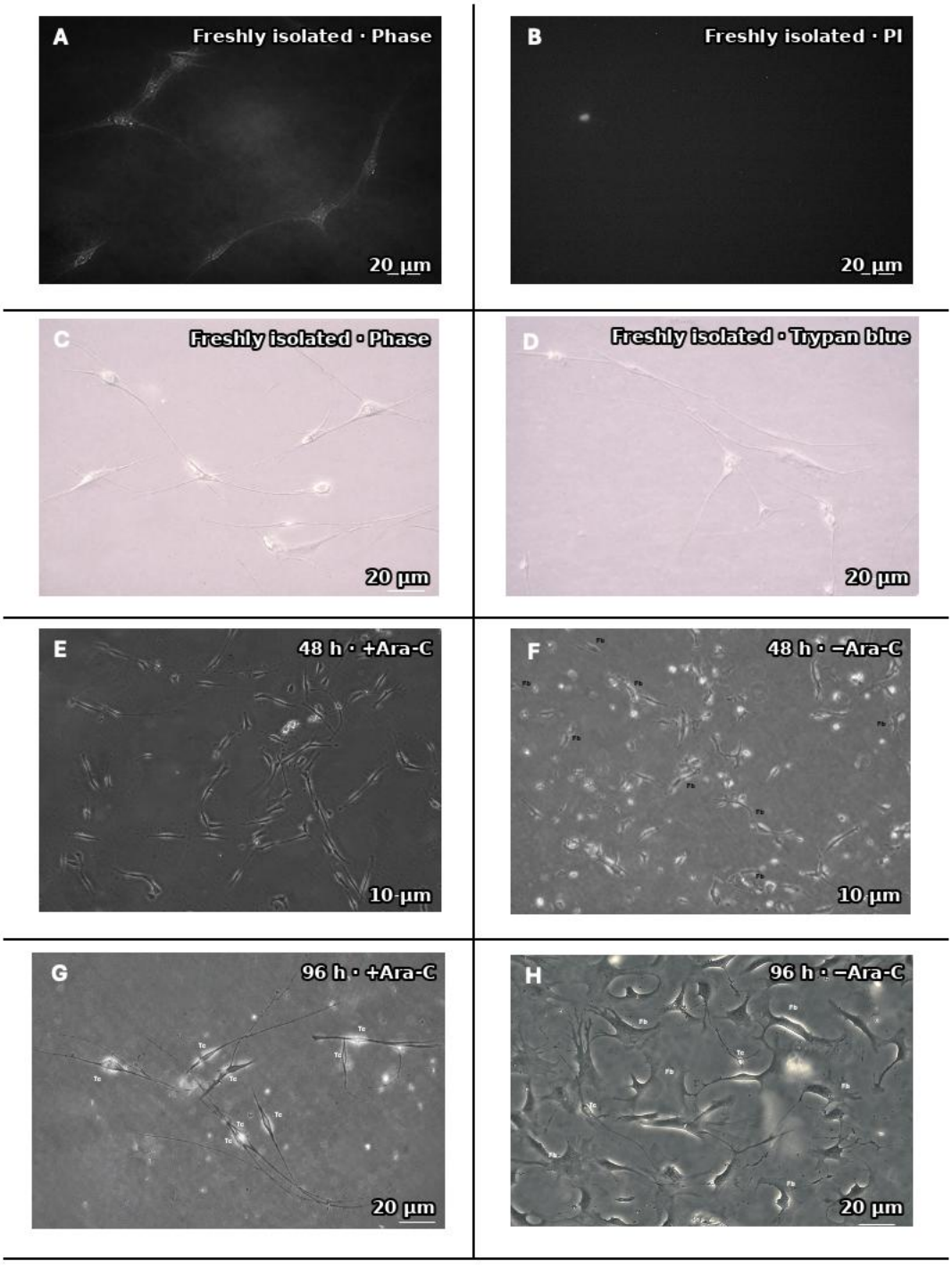
3. Viability and Culture Stability of Isolated Telocyte-Like Cells

Cell viability and short-term culture stability were assessed using propidium iodide (PI) staining, Trypan blue exclusion, and phase-contrast microscopy. Immediately after isolation,

representative PI and Trypan blue assays indicated preserved membrane integrity in telocyte-like cells following the isolation procedure (Fig. 4A–D).

During short-term culture, cells adhered to the culture substrate and developed the elongated morphology described above. At 48 h, telocyte-like cells displaying elongated cytoplasmic processes were observed in both Ara-C-treated and untreated cultures, while Ara-C-treated cultures qualitatively appeared to contain fewer fibroblast-like cells (Fig. 4E, F).

After 96 h, Ara-C-treated cultures continued to contain telocyte-like cells with elongated cell bodies and well-defined telopode-like processes and qualitatively showed less fibroblast-like cell overgrowth than untreated cultures (Fig. 4G, H). Representative PI staining and Trypan blue exclusion performed after 96 h of Ara-C exposure indicated preservation of membrane integrity in the cultured telocyte-like cells (Fig. 4I–L).


A
Freshly isolated · Phase
20 µm
B
Freshly isolated · PI
20 µm
C
Freshly isolated · Phase
20 µm
D
Freshly isolated · Trypan blue
20 µm
E
48 h · +Ara-C
10 µm
F
48 h · −Ara-C
10 µm
G
96 h · +Ara-C
20 µm
H
96 h · −Ara-C
20 µm

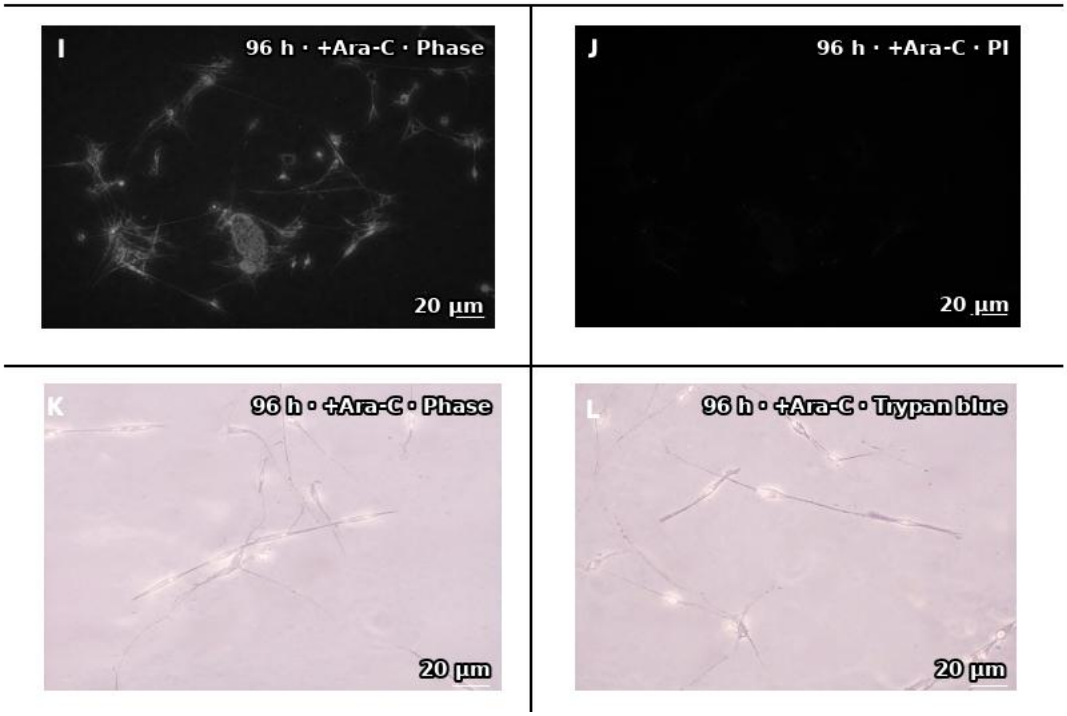


Figure 4. Viability and short-term culture stability of isolated telocyte-like cells. (A, B) Representative phase-contrast and corresponding propidium iodide (PI) images of freshly isolated telocyte-like cells. (C, D) Representative phase-contrast image and corresponding Trypan blue exclusion assay of freshly isolated telocyte-like cells. (E, F) Representative cultures maintained for 48 h in the presence (+Ara-C) or absence (−Ara-C) of Ara-C, respectively. (G, H) Representative cultures maintained for 96 h in the presence (+Ara-C) or absence (−Ara-C) of Ara-C, respectively. (I, J) Representative phase-contrast and corresponding PI images of Ara-C-treated telocyte-like cells after 96 h of culture. (K, L) Representative phase-contrast image and corresponding Trypan blue exclusion assay of Ara-C-treated telocyte-like cells after 96 h of culture. Culture duration, Ara-C treatment condition, and imaging modality or viability assay are indicated directly on the corresponding panels. Panels A–D and G–L were acquired using a 20× objective (scale bars = 20 µm). Panels E and F were acquired using a 20× objective (scale bars = 10 µm).

4. Periganglionic Localization of Telocyte-Like Cells Within the Intrinsic Cardiac Nervous System

To examine the anatomical localization of telocyte-like cells within the intrinsic cardiac ganglionic region, tissue sections containing intracardiac ganglia were analyzed by confocal immunofluorescence. Elongated CD34-positive stromal cells were observed within the connective tissue surrounding PGP9.5-positive intrinsic cardiac neurons and nerve fibers (Fig. 5).

Confocal Z-stack projections revealed CD34-positive cells with long, slender processes extending around neuronal cell bodies and along neural structures. Higher-magnification reconstructions further demonstrated the close spatial association between CD34-positive telopode-like processes and PGP9.5-positive intrinsic cardiac neurons and nerve fibers. α-SMA immunolabeling identified adjacent smooth muscle structures and provided additional anatomical context for the organization of the periganglionic region.

Together, these observations demonstrate the presence of elongated CD34-positive telocyte-like stromal cells in close spatial association with neural structures within the intrinsic cardiac ganglionic microenvironment.

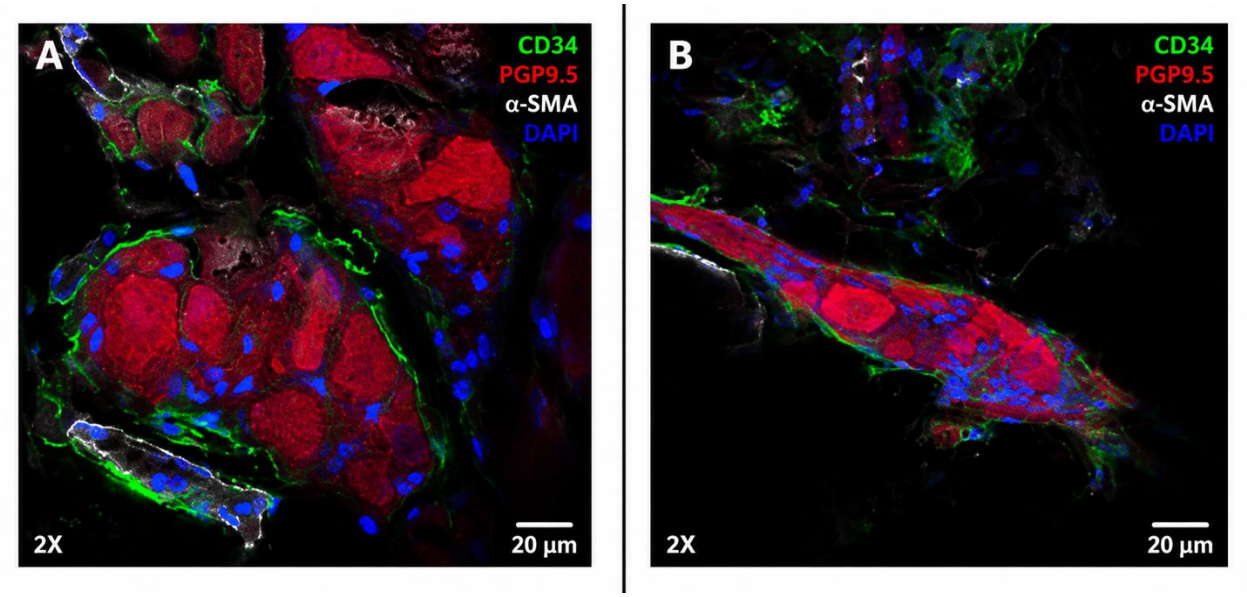


Figure 5. Periganglionic localization of CD34-positive telocyte-like cells within the intrinsic cardiac nervous system. (A) Confocal Z-stack projection showing elongated CD34-positive stromal cells (green) surrounding PGP9.5-positive intrinsic cardiac neurons and nerve fibers (red). α-SMA immunoreactivity (white) identifies adjacent smooth muscle structures. (B) Higher-magnification confocal Z-stack projection illustrating the close spatial association between CD34-positive telopode-like processes, PGP9.5-positive neuronal cell bodies and nerve fibers, and adjacent α-SMA-positive structures. Images were acquired using a 20× objective with a 2× digital zoom. Scale bars = 20 µm.

5. Representative Regional Distribution of CD34-Positive Cells Throughout the Rat Heart

Representative regional mapping demonstrated elongated CD34-positive interstitial cells within the connective tissue surrounding the intracardiac ganglia (Fig. 6). Elongated CD34-positive cells were also observed in non-ganglionic atrial myocardium, upper and lower ventricular myocardium, and the cardiac apex.

Within the intracardiac ganglionic region, CD34-positive cells were observed in the connective tissue surrounding the ganglia, whereas in the myocardial regions examined, CD34-positive interstitial cells displayed a more dispersed distribution. Because this analysis was performed as a qualitative anatomical assessment in two rat hearts, no conclusions regarding regional differences in cell abundance or density were drawn.

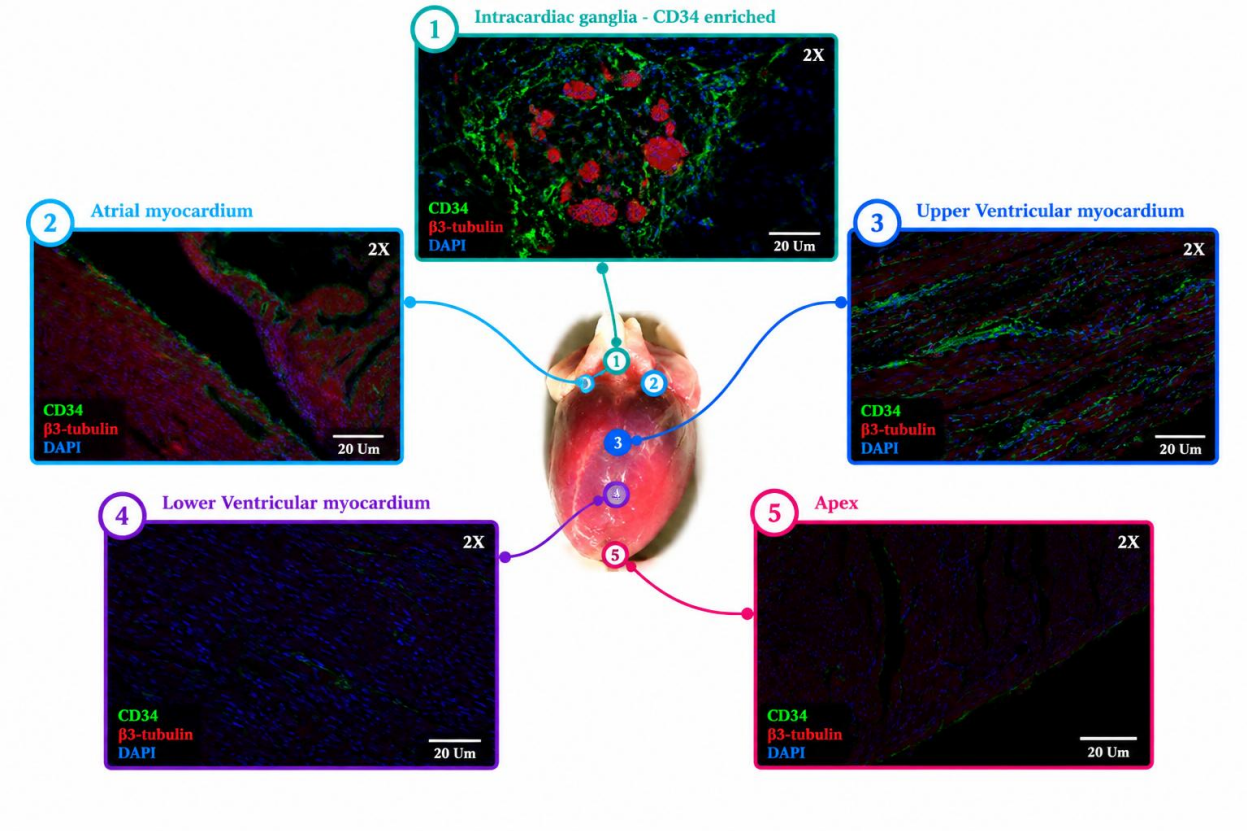


Figure 6. Representative regional distribution of CD34-positive interstitial cells throughout the rat heart. Representative confocal images showing elongated CD34-positive interstitial cells (green) in the intracardiac ganglionic region, non-ganglionic atrial myocardium, upper ventricular myocardium, lower ventricular myocardium, and cardiac apex. Nuclei were counterstained with DAPI (blue). Images are representative of qualitative regional mapping performed in two rat hearts. No quantitative regional cell-density analysis or inferential statistical comparison was performed.

6. Functional Calcium-Dependent Fluorescence Responses of Isolated Telocyte-Like Cells

Functional responsiveness of isolated telocyte-like cells was assessed using Fluo-4 AM-based live-cell calcium imaging following stimulation with angiotensin II or caffeine.

Angiotensin II-evoked responses were analyzed in 46 cells obtained from cultures derived from eight independent animals. Angiotensin II increased Ca^{2+}-dependent fluorescence in all 46 analyzed cells (46/46, 100%). No cells were excluded from the analysis based on response magnitude, and no additional post hoc responder threshold was applied. Paired analysis demonstrated a significant increase in fluorescence amplitude from 26.0 ± 0.9 a.u. at baseline to 31.6 ± 1.1 a.u. following stimulation ($P < 0.0001$, Wilcoxon matched-pairs signed-rank test; Fig. 7A). Representative normalized Fluo-4 recordings showed a rapid increase following angiotensin II application, with maximal responses occurring approximately 20–40 s after stimulation and followed by a sustained elevation above prestimulation levels in the representative recordings shown (Fig. 7B).

Caffeine-evoked responses were analyzed in 21 cells obtained from cultures derived from eight independent animals. Caffeine increased Ca^{2+}-dependent fluorescence in all 21 analyzed cells (21/21, 100%). As for angiotensin II, no cells were excluded based on response magnitude and no additional post hoc responder threshold was applied. Paired analysis demonstrated a significant increase in fluorescence amplitude from 21.8 ± 1.6 a.u. at baseline to 30.4 ± 3.8 a.u. following caffeine stimulation ($P < 0.0001$, Wilcoxon matched-pairs signed-rank test; Fig. 7C). Representative normalized recordings showed a rapid increase in Ca^{2+}-dependent fluorescence, with maximal responses occurring approximately 5–15 s after stimulation and followed by a progressive decline toward prestimulation levels in the representative recordings shown (Fig. 7D).

Normalized response amplitudes ($\Delta F/F_0$) were additionally examined to provide a descriptive comparison of the responses elicited by angiotensin II and caffeine (Fig. 7E). Both stimuli produced variable increases in normalized Ca^{2+}-dependent fluorescence across individual cells. These data are presented descriptively, and no inferential statistical comparison between angiotensin II and caffeine was performed.

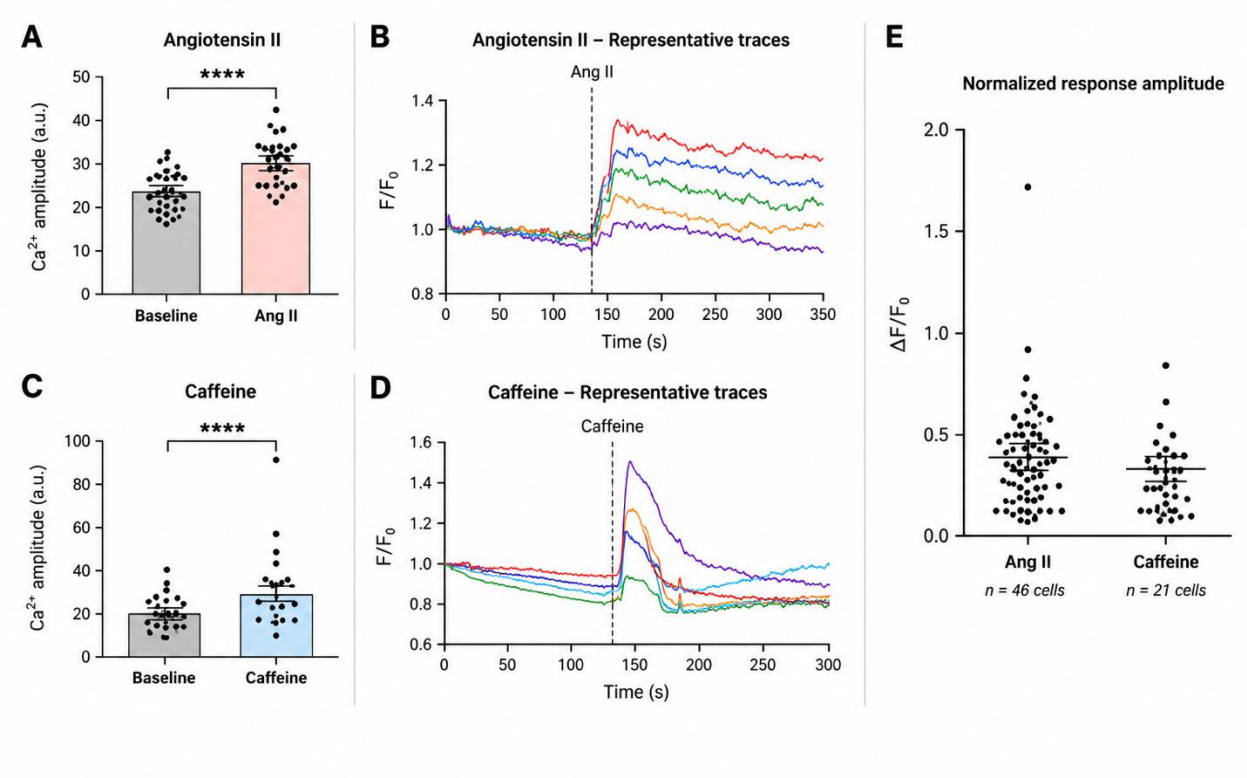


Figure 7. Angiotensin II- and caffeine-evoked calcium-dependent fluorescence responses in isolated telocyte-like cells. (A) Paired quantification of Fluo-4 fluorescence amplitude during the prestimulation baseline and following angiotensin II stimulation. Each paired observation represents one analyzed cell (n = 46 cells from cultures derived from 8 independent animals). Angiotensin II significantly increased fluorescence amplitude from 26.0 ± 0.9 to 31.6 ± 1.1 a.u. (Wilcoxon matched-pairs signed-rank test, $P < 0.0001$). (B) Representative normalized Fluo-4 fluorescence recordings before and after angiotensin II stimulation. The dashed vertical line indicates agonist application. In the representative recordings shown, maximal responses occurred approximately 20-40 s after stimulation and were followed by a sustained elevation above baseline. (C) Paired quantification of Fluo-4 fluorescence amplitude during the prestimulation baseline and following caffeine stimulation. Each paired observation represents one analyzed cell (n = 21 cells from cultures derived from 8 independent animals). Caffeine significantly increased fluorescence amplitude from 21.8 ± 1.6 to 30.4 ± 3.8 a.u. (Wilcoxon matched-pairs signed-rank test, $P < 0.0001$). (D) Representative normalized Fluo-4 fluorescence recordings before and after caffeine stimulation. In the representative recordings shown, maximal responses occurred approximately 5–15 s after stimulation and were followed by a progressive decline toward prestimulation levels. (E) Descriptive comparison of normalized response amplitudes ($\Delta F/F_0$) following angiotensin II and caffeine stimulation. Each symbol represents one analyzed cell. Horizontal lines and error bars represent mean ± SEM. No inferential statistical comparison between angiotensin II and caffeine was performed.

Discussion

The present study describes an anatomically targeted approach for the isolation and characterization of telocyte-like cells from the intracardiac ganglionic region of the rat heart. By combining microdissection of the dorsal atrial ganglionic region with sequential enzymatic dissociation and short-term primary culture, we obtained cells displaying characteristic telocyte-like morphology, including elongated moniliform processes with alternating podomers and podoms. These cells expressed the telocyte-associated markers CD34, PDGFRα, and vimentin, while confocal analysis of cardiac tissue demonstrated elongated CD34-positive stromal cells in close spatial association with intracardiac neurons and nerve fibers. The isolated cells also exhibited Ca^{2+}-dependent fluorescence responses to angiotensin II and caffeine, demonstrating that pharmacologically evoked calcium signaling was retained following isolation and short-term culture. Together, these findings establish a regionally targeted experimental approach for investigating periganglionic cardiac telocyte-like cells and provide a basis for future studies of neuro-stromal interactions within the intrinsic cardiac nervous system.

Cardiac telocytes have been described in several anatomical compartments of the heart, including the epicardium, endocardium, myocardium, valves, and perivascular connective tissue, and have been proposed to participate in tissue organization, intercellular communication, extracellular matrix regulation, and regenerative processes[13,15]. Despite growing interest in cardiac telocytes, comparatively little attention has been directed toward telocyte-like stromal cells associated with the intrinsic cardiac nervous system. Intracardiac ganglia form part of a specialized cardiac neural network containing neuronal cell bodies, nerve fibers, glial elements, vascular structures, extracellular matrix, and surrounding stromal components[12–14]. In the present study, elongated CD34-positive stromal cells were observed in close spatial association with PGP9.5-positive neurons and nerve fibers within this compartment. Importantly, the regional mapping performed here was qualitative and does not establish a greater abundance of CD34-positive cells in the ganglionic region than in other cardiac regions. Rather, these findings identify the intracardiac ganglionic region as an anatomically defined source from which telocyte-like stromal cells can be specifically investigated [15].

A principal methodological feature of the present study is the use of anatomical targeting before tissue dissociation. Previous approaches to cardiac telocyte isolation have relied on enzymatic dissociation of cardiac tissue followed by primary culture and, in some protocols, additional enrichment or purification procedures[7,15]. Li et al., for example, isolated cardiac telocytes by enzymatic digestion and subsequently used CD34/PDGFRα-based flow-cytometric sorting followed by immunofluorescence and ultrastructural characterization[7]. In contrast, microdissection of the ganglion-containing dorsal atrial region in the present study restricts the starting material to a defined anatomical compartment before enzymatic and mechanical dissociation. The subsequent combination of collagenase/Dispase digestion, controlled trypsinization, gentle mechanical trituration, and short-term primary culture yielded telocyte-like cells displaying characteristic elongated, moniliform processes across the independent preparations examined. The approach does not eliminate the possibility that other stromal populations are present in culture and should therefore not be regarded as a purification method. Rather, its principal advantage is the ability to investigate telocyte-like cells originating from a

defined cardiac microenvironment without requiring cell sorting or other additional enrichment procedures.

Reliable identification of telocytes remains a major methodological challenge because no single molecular marker is considered sufficiently specific to establish telocyte identity independently of morphology and anatomical context[3,15]. Cardiac telocytes have been reported to express several stromal markers, including CD34, PDGFRα, PDGFRβ, and vimentin, although their expression profiles may vary and overlap with those of other interstitial cell populations[8,9,15]. In particular, CD34/PDGFRα co-expression has been demonstrated in cultured cardiac telocytes and proposed as a useful combination for their immunophenotypic characterization[9]. Li et al. similarly used CD34 and PDGFRα for purification of rat cardiac telocytes and demonstrated vimentin expression in the resulting population[7]. Marker expression alone, however, remains insufficient to establish telocyte identity.

For this reason, characterization in the present study was based on the integration of anatomical origin, cellular morphology, and immunophenotypic labeling. Cultured cells displayed compact cell bodies and long, thin, moniliform processes containing alternating podomer- and podom-like regions and expressed CD34, PDGFRα, and vimentin. Cells with broad or flattened cell bodies and short, thick processes characteristic of fibroblast-like morphology were excluded from telocyte-specific analyses. In parallel, elongated CD34-positive stromal cells with telopode-like processes were visualized in situ within the connective tissue surrounding intracardiac ganglia. This multimodal approach is consistent with current recommendations emphasizing the integration of morphological and molecular criteria when studying telocytes[15]. The combined morphological, immunophenotypic, and anatomical evidence therefore supports classification of the isolated cells as telocyte-like cells while recognizing the absence of a uniquely specific molecular marker and ultrastructural confirmation.

Short-term culture experiments further indicated that the isolated telocyte-like cells remained morphologically identifiable following the dissociation procedure. Representative PI staining and Trypan blue exclusion supported preservation of membrane integrity immediately after isolation and during short-term culture. Ara-C was additionally evaluated as an optional antimitotic treatment to limit the expansion of fibroblast-like cells. Cultures exposed to Ara-C qualitatively appeared to contain less fibroblast-like overgrowth while retaining cells with telocyte-like morphology for up to 96 h. However, these observations were qualitative, and the present experiments were not designed to quantify differences in telocyte viability, fibroblast abundance, or culture purity between Ara-C-treated and untreated conditions. Ara-C should therefore be regarded as an optional culture-stabilization step rather than a validated method for selective telocyte enrichment.

The demonstration of pharmacologically evoked Ca^{2+}-dependent fluorescence responses provides an additional functional dimension to the characterization of the isolated cells. Calcium signaling is involved in numerous cellular processes, and dynamic intracellular Ca^{2+} signaling has been described in telocytes and other interstitial cell populations[10]. Previous studies have identified several mechanisms capable of contributing to telocyte Ca^{2+} dynamics, including membrane-associated calcium channels and mobilization of intracellular calcium stores[16]. In the present study, angiotensin II significantly increased Fluo-4 fluorescence in all 46 analyzed cells,

while caffeine significantly increased fluorescence in all 21 analyzed cells. Representative normalized recordings showed different temporal profiles: angiotensin II stimulation was followed by a relatively sustained post-peak elevation, whereas caffeine produced a faster response followed by a more pronounced decline toward prestimulation levels. These observations demonstrate that telocyte-like cells isolated from the intracardiac ganglionic region retain responsiveness to distinct pharmacological stimuli following short-term culture.

The calcium-imaging experiments were not designed to establish mechanistic differences between angiotensin II- and caffeine-dependent signaling. Although normalized response amplitudes were displayed descriptively, no inferential statistical comparison between the two stimuli was performed, and the representative temporal recordings should not be interpreted as population-level kinetic analyses. The complexity of calcium signaling previously described in telocytes further argues against attributing the observed responses to a single pathway without direct pharmacological evidence[10]. The present experiments therefore do not establish the specific receptors, intracellular stores, membrane channels, or downstream signaling pathways responsible for the observed responses. Future studies combining pharmacological inhibition with population-level kinetic analyses could determine the relative contributions of extracellular Ca^{2+} entry and intracellular Ca^{2+} mobilization and identify the molecular pathways underlying these responses in periganglionic telocyte-like cells.

The anatomical relationship between telocyte-like stromal cells and intracardiac neural structures raises further questions regarding their potential role within the intrinsic cardiac nervous system. Telocytes form extensive interstitial networks and have been proposed to participate in local cellular communication through direct contacts, paracrine signaling, and extracellular vesicles[3,6]. The intrinsic cardiac nervous system comprises interconnected intracardiac ganglia and neuronal networks that integrate local and extrinsic autonomic inputs and contribute to the modulation of cardiac electrophysiology and function[12,13]. In the present study, elongated CD34-positive cells and their processes were observed in close spatial association with PGP9.5-positive neuronal cell bodies and nerve fibers. Spatial proximity alone does not demonstrate functional communication; nevertheless, the localization of these cells within the periganglionic microenvironment provides an anatomical basis for investigating potential neuro-stromal interactions. Such interactions could involve regulation of the local extracellular matrix, modulation of the neuronal microenvironment, or coordination of stromal responses to physiological or pathological stimuli. Direct functional experiments will be required to determine whether periganglionic telocyte-like cells influence intrinsic cardiac neurons or other components of this specialized microenvironment.

This experimental platform may also be relevant to the study of cardiac remodeling and disease. Alterations in telocyte networks have been associated with pathological conditions in several tissues, and growing evidence has stimulated interest in their potential contributions to tissue remodeling and repair[15]. In parallel, dysfunction and remodeling of the intrinsic cardiac nervous system have been implicated in autonomic imbalance, abnormal cardiac electrophysiology, and arrhythmogenesis[12,13]. The ability to obtain telocyte-like cells from an anatomically defined ganglionic region therefore creates an opportunity to examine whether this stromal population undergoes phenotypic or functional remodeling under pathological conditions. Future studies could compare cells isolated from healthy and diseased hearts and examine changes in

morphology, calcium signaling, secretory profiles, extracellular-matrix interactions, and communication with intrinsic cardiac neurons. Such experiments would be required before assigning a direct role to periganglionic telocytes in autonomic dysfunction, fibrosis, or other forms of adverse cardiac remodeling.

Several limitations should be considered when interpreting these findings. First, transmission electron microscopy was not performed. Ultrastructural analysis remains an important component of rigorous telocyte characterization because it permits detailed visualization of the characteristic telopodal architecture[3,15]. Although the moniliform processes observed by phase-contrast and confocal microscopy, together with the immunophenotypic and anatomical findings, support a telocyte-like phenotype, ultrastructural confirmation would provide stronger evidence of telocyte identity. Second, CD34, PDGFRα, and vimentin are not uniquely specific for telocytes[8,9,15], and the presence of other stromal populations in the primary cultures cannot be excluded. Third, regional CD34 mapping was performed qualitatively in two hearts and was not designed to establish differences in telocyte abundance or density among cardiac regions. Fourth, the viability and Ara-C experiments were representative and qualitative and therefore do not establish quantitative effects on cell survival or culture composition. Fifth, functional characterization was limited to Fluo-4-based calcium imaging following angiotensin II and caffeine stimulation. No prospectively defined quantitative responder threshold was applied, and temporal response characteristics were evaluated from representative recordings rather than through population-level kinetic analysis.

Finally, individual cells constituted the observational units for the paired calcium-response analyses, with multiple cells obtained from cultures derived from the same animals. Because cell-level measurements were not analyzed using an animal-level hierarchical or mixed-effects framework, the reported statistical comparisons should be interpreted as evidence of paired cellular responses rather than as independent animal-level estimates. Future studies incorporating ultrastructural analysis, quantitative regional mapping, hierarchical experimental designs, electrophysiology, pharmacological pathway interrogation, transcriptomic or proteomic profiling, secretome analysis, and co-culture with intrinsic cardiac neurons would provide a more comprehensive characterization of this cell population.

Conclusion

In summary, this study presents an anatomically targeted approach for isolating and characterizing telocyte-like cells from the intracardiac ganglionic region of the rat heart. The isolated cells displayed characteristic telocyte-like morphology, expressed CD34, PDGFRα, and vimentin, and exhibited pharmacologically evoked Ca^{2+}-dependent fluorescence responses to angiotensin II and caffeine. Complementary tissue imaging demonstrated elongated CD34-positive stromal cells in close spatial association with components of the intrinsic cardiac nervous system, supporting the anatomical relevance of the targeted isolation region.

By combining regional microdissection with morphological, immunophenotypic, anatomical, and functional characterization, this approach provides an experimental platform for studying periganglionic cardiac telocyte-like cells without requiring additional cell-sorting procedures. Further studies incorporating ultrastructural validation and mechanistic analyses will be required

to define their cellular identity more precisely and determine their functional relationships with intrinsic cardiac neurons. The present work therefore provides a methodological foundation for future investigation of telocyte biology and neuro-stromal interactions within the cardiac ganglionic microenvironment.

Acknowledgements

The authors gratefully acknowledge Anna Maria Bramili and Alice Jean for their valuable technical and laboratory support at the Laboratory of Research in Physiology and Pathophysiology (LRPP), Saint Joseph University of Beirut, and the PRéTI Laboratory, University of Poitiers, respectively. The authors also acknowledge the ImageUP and PREBIOS platforms of the University of Poitiers for providing access to facilities and technical resources that supported this work.

Author Contributions

J.-A.G. conceived and conducted the study, performed the experiments and data analysis, and wrote the original manuscript. Y.S. contributed to manuscript preparation and writing. C.S. contributed to the experimental work. P.B., A.C., and N.F. supervised the study and critically reviewed and revised the manuscript. All authors contributed to the interpretation and discussion of the findings, reviewed the manuscript, and approved the final version for submission.

Funding

This work was supported by the Partenariat Hubert Curien (PHC) CEDRE program (Grant No. 50498SG), within the framework of the scientific collaboration between Saint Joseph University of Beirut, Lebanon, and the University of Poitiers, France, and by the Research Council of Saint Joseph University of Beirut (Project No. FM481). This work also benefited from support from the UP-SQUARED program of the French National Research Agency (ANR-21-EXES-0013) and the Fondation de France (FDF; 00158937 / WB-2024-55345).

Data Availability

The datasets generated and/or analysed during the current study are available from the corresponding author on reasonable request.

Competing Interests

The authors declare no competing interests.

Ethics Approval

All animal procedures were approved by the Ethics Committee of Saint Joseph University of Beirut (approval no. USJ-2023-314) and were conducted in accordance with the Guiding Principles for the Care and Use of Animals established by the American Physiological Society and European Parliament Directive 2010/63/EU.

References

1. Varga, I. *et al.* Recently discovered interstitial cells termed telocytes: distinguishing cell-biological and histological facts from fictions. *Biologia (Bratisl.)* **74**, 195–203 (2019).
2. Popescu, L. M. & Faussone-Pellegrini, M.-S. TELOCYTES - a case of serendipity: the winding way from Interstitial Cells of Cajal (ICC), via Interstitial Cajal-Like Cells (ICLC) to TELOCYTES. *J. Cell. Mol. Med.* **14**, 729–740 (2010).
3. Cretoiu, S. M. & Popescu, L. M. Telocytes revisited. *Biomol. Concepts* **5**, 353–369 (2014).
4. Tao, L., Wang, H., Wang, X., Kong, X. & Li, X. Cardiac Telocytes. *Curr. Stem Cell Res. Ther.* **11**, 404–409 (2016).
5. Varga, I. *et al.* The functional morphology and role of cardiac telocytes in myocardium regeneration. *Can. J. Physiol. Pharmacol.* **94**, 1117–1121 (2016).
6. Yang, J., Li, Y., Xue, F., Liu, W. & Zhang, S. Exosomes derived from cardiac telocytes exert positive effects on endothelial cells. *Am. J. Transl. Res.* **9**, 5375–5387 (2017).
7. Li, Y.-Y., Zhang, S., Li, Y.-G. & Wang, Y. Isolation, culture, purification and ultrastructural investigation of cardiac telocytes. *Mol. Med. Rep.* **14**, 1194–1200 (2016).
8. Chang, Y., Li, C., Lu, Z., Li, H. & Guo, Z. Multiple immunophenotypes of cardiac telocytes. *Exp. Cell Res.* **338**, 239–244 (2015).
9. Zhou, Q. *et al.* Cardiac telocytes are double positive for CD34/PDGFR-α. *J. Cell. Mol. Med.* **19**, 2036–2042 (2015).

10. Radu, B. M. *et al.* Calcium Signaling in Interstitial Cells: Focus on Telocytes. *Int. J. Mol. Sci.* **18**, 397 (2017).
11. Gemayel, J.-A., Chatelier, A., Bois, P. & Fares, N. The Heart's Hidden Neural Network: Interplay Between Intracardiac Ganglia, Fibrosis and Cardiac Remodeling. *Int. J. Mol. Sci.* https://doi.org/10.3390/ijms27031582 (2026).
12. Fedele, L. & Brand, T. The Intrinsic Cardiac Nervous System and Its Role in Cardiac Pacemaking and Conduction. *J. Cardiovasc. Dev. Dis.* **7**, 54 (2020).
13. Giannino, G. *et al.* The Intrinsic Cardiac Nervous System: From Pathophysiology to Therapeutic Implications. *Biology* **13**, 105 (2024).
14. Lizot, G. *et al.* Molecular and functional characterization of the mouse intrinsic cardiac nervous system. *Heart Rhythm* **19**, 1352–1362 (2022).
15. Sanches, B. D. A. *et al.* Telocytes: current methods of research, challenges and future perspectives. *Cell Tissue Res.* **396**, 141–155 (2024).
16. Calcium Signaling in Interstitial Cells: Focus on Telocytes - PMC. https://pmc.ncbi.nlm.nih.gov/articles/PMC5343932/.